A four-dimensional chaotic spiking oscillator

Yusuke Takahashi, Hidehiro Nakano and Toshimichi Saito
Department of Electronics, Electrical and Computer Engineering, Faculty of Engineering,
HOSEI University, 3-7-2, Kajino-cho, Koganei-shi, Tokyo, 184-8584, JAPAN
Tel.: +81-42-387-6204, Fax.: +81-42-387-6122
E-mail: yusuke@nonlinear.k.hosei.ac.jp

Abstract: This paper presents a novel 4-D chaotic spiking oscillator. The oscillator can generate hyperchaos characterized by two positive Lyapunov exponents. Using a simple test circuit, typical phenomena can be verified in the laboratory.

1. Introduction

The spiking oscillator is known as simple and interesting circuit, and have been studied intensively. Fig.1 shows the spiking oscillator consists of N-D linear oscillator and spiking switch. The switch is characterized by "If the capacitor voltage v reaches a threshold, the switch S is closed and v is reset to the base voltage E, instantaneously." The switching jump corresponds to the $(N+1)$th state. Therefore, the circuit is $(N+1)$ dimensional. In the existing works, a 2-D spiking oscillator relates to a simple neuron model that exhibits periodic phenomena only [1]. In our previous works, we have studied 3-D chaotic spiking oscillators (ab. CSOs) which can exhibit chaos and bifurcation phenomena [2].

In this paper, we present a novel 4-D chaotic spiking oscillator. The four or more dimensional system exhibits interesting complicated phenomena such as hyperchaos [3][4]. We can expect that the 4-D CSO can exhibit rich phenomena that the 3-D CSOs can not exhibit. Since the 4-D CSO is piecewise linear, the dynamics is described by the 2-D return map which is given theoretically. Using this map, Lyapunov exponent can be calculated precisely. Analysis of these phenomena is important as basic nonlinear problems such as classification of chaos and bifurcation phenomena. It also relates to engineering applications such as the pulse-coupled neural networks for information processing [5][6].

Next we present a simple implementation circuit of the 4-D CSO. The circuit consists of three capacitors, three Operational Transconductance Amplifiers (ab. OTAs), one comparator, one pulse generator (ab. P.G.) and one spiking switch. Using a simple test circuit, typical phenomena can be verified in the laboratory.

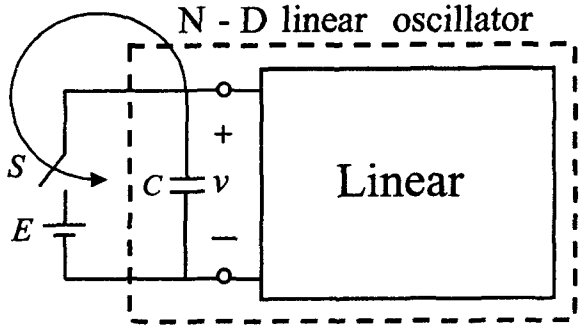

Figure 1. A circuit family of the spiking oscillator.

2. 4-D chaotic spiking oscillator

Fig.2 shows the implementation example of the 4-D CSO. In the figure the OTAs are voltage-controlled current sources converting the input differential voltage into the output current, e.g., $i_1 = g_1 v_3$. Three OTAs construct a three-port voltage controlled current source (ab. 3PVCCS). Typical phenomena can be verified in the laboratory. Connecting three capacitors to the three ports, we obtain a linear circuit described by Equation (1) if the switched S is opened

$$\frac{d}{dt}\begin{bmatrix} C_1 v_1 \\ C_2 v_2 \\ C_3 v_3 \end{bmatrix} = \begin{bmatrix} 0 & 0 & g_1 \\ 0 & g_2 & -g_2 \\ -g_3 & g_3 & 0 \end{bmatrix} \begin{bmatrix} v_1 \\ v_2 \\ v_3 \end{bmatrix}, \quad (1)$$

$$\text{for } v_1(t) < V_T.$$

If the capacitor voltage v_1 reaches a threshold voltage V_T, the switch S is closed and v_1 is reset to a base voltage $E(< V_T)$ instantaneously, holding (v_2, v_3)=constant. The switching rule is described by Equation (2).

$$\begin{bmatrix} v_1(t^+) \\ v_2(t^+) \\ v_3(t^+) \end{bmatrix} = \begin{bmatrix} E \\ v_2(t) \\ v_3(t) \end{bmatrix}, \quad (2)$$

$$\text{if } v_1(t) = V_T.$$

Here, we assume that the matrix of Equation (1) has a real eigenvalue $\lambda\omega$ and complex conjugate eigenvalues $\delta\omega \pm j\omega$. δ, ω, λ are given by Equation (3).

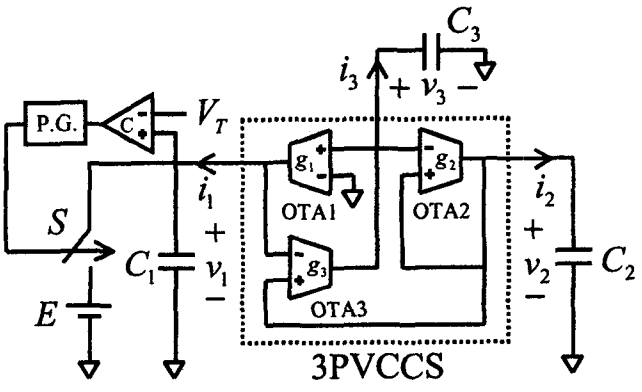

Figure 2. Implementation example of the 4-D CSO.

$$\lambda(\delta^2+1)\omega^3 = \frac{g_1 g_2 g_3}{C_1 C_2 C_3},$$
$$(2\delta\lambda+\delta^2+1)\omega^2 = \frac{g_1 g_3}{C_1 C_3} + \frac{g_2 g_3}{C_2 C_3}, \quad (3)$$
$$(2\delta+\lambda)\omega = \frac{g_2}{C_2},$$

where we assume $\delta > 0$, $\lambda > 0$ and $\omega > 0$. Using the following dimensionless variables and parameters:

$$\tau = \omega t, \ \frac{1}{V_T}\boldsymbol{v} = \boldsymbol{A}\boldsymbol{u}, \ \boldsymbol{e}_1 = \boldsymbol{A}\boldsymbol{p}, \ q = \frac{E}{V_T}, \quad (4)$$
$$\boldsymbol{v} = [v_1, v_2, v_3]^T, \quad \boldsymbol{u} = [u_1, u_2, u_3]^T,$$
$$\boldsymbol{e}_1 = [1, 0, 0]^T, \quad \boldsymbol{p} = [1 - p_3, p_2, p_3]^T,$$
$$\boldsymbol{A} = \begin{bmatrix} 1 & 0 & 0 \\ 1 & 0 & 1 \\ -\frac{g_3}{g_1}\frac{C_1}{C_3} & \frac{g_3}{g_1}\frac{C_1}{C_3} & 0 \end{bmatrix}^{-1}$$
$$\times \begin{bmatrix} 1 & 0 & 1 \\ \frac{\delta\omega C_1}{g_1} & \frac{\omega C_1}{g_1} & \frac{\lambda\omega C_1}{g_1} \\ (\delta^2-1)(\frac{\omega C_1}{g_1})^2 & 2\delta(\frac{\omega C_1}{g_1})^2 & (\frac{\lambda\omega C_1}{g_1})^2 \end{bmatrix},$$

Equations (1) and (2) are transformed into Equations (5) and (6).

$$\frac{d}{d\tau}\begin{bmatrix} u_1 \\ u_2 \\ u_3 \end{bmatrix} = \begin{bmatrix} \delta & 1 & 0 \\ -1 & \delta & 0 \\ 0 & 0 & \lambda \end{bmatrix}\begin{bmatrix} u_1 \\ u_2 \\ u_3 \end{bmatrix}, \quad (5)$$
$$\text{for } u_1(\tau) + u_3(\tau) < 1,$$

$$\begin{bmatrix} u_1(\tau^+) \\ u_2(\tau^+) \\ v_3(\tau^+) \end{bmatrix} = \begin{bmatrix} u_1(\tau) - (1-p_3)(1-q) \\ u_2(\tau) - p_2(1-q) \\ u_3(\tau) - p_3(1-q) \end{bmatrix}, \quad (6)$$
$$\text{if } u_1(\tau) + u_3(\tau) = 1.$$

The 4-D CSO have five parameters: $\delta, \lambda, p_2, p_3, q$. For simplicity, we choose the base level q as the control parameter and fix the other parameters as the followings:

$$\delta = 0.02, \ \lambda = 0.04, \ p_2 = -0.03, \ p_3 = 0.5.$$

The trajectory moves as illustrated in Fig.3. The trajectory rotates divergently around the u_3 axis. If the trajectory reaches a threshold plane $u_1 + u_3 = 1$, it jumps onto the base plane $u_1 + u_3 = q$ along the direction vector $(1 - p_3, p_2, p_3)^T$ instantaneously. Equation (5) has the following exact piecewise solution.

$$\begin{bmatrix} u_1(\tau) \\ u_2(\tau) \\ u_3(\tau) \end{bmatrix} = e^{\delta\tau}\begin{bmatrix} \cos\tau & \sin\tau & 0 \\ -\sin\tau & \cos\tau & 0 \\ 0 & 0 & e^{(\lambda-\delta)\tau} \end{bmatrix} \quad (7)$$
$$\times \begin{bmatrix} u_1(0) \\ u_2(0) \\ u_3(0) \end{bmatrix}, \text{ for } u_1(\tau) + u_3(\tau) < 1.$$

where, $(u_1(0), u_2(0), u_3(0))^T$ denotes an initial state vector at $\tau = 0$.

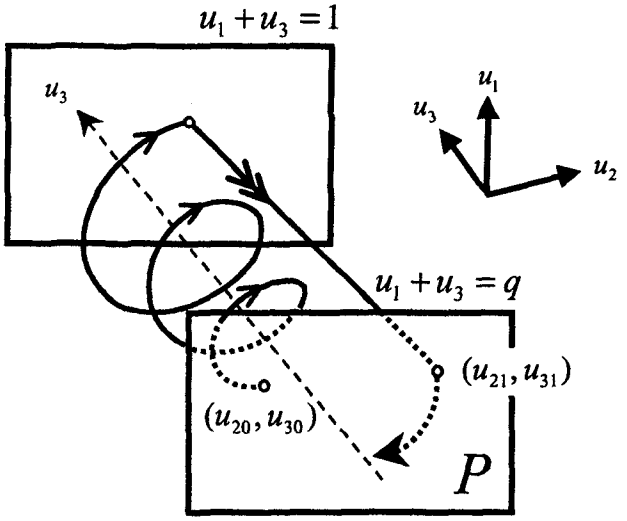

Figure 3. Phase space.

3. 2-D return map

In order to derive a 2-D return map, we define a plane

$$P \equiv \{(u_1, u_2, u_3) | u_1 = q - u_3\}. \quad (8)$$

Let a point on P be represented by its u_2-u_3-coordinate. As an orbit starts from a point (u_{20}, u_{30}) on P at $\tau = 0$, it must reach the threshold at some positive time $\tau = \tau_0$. At this moment the orbit jumps and returns to a point (u_{21}, u_{31}) on P (see Fig.3). Then we can define the following 2-D return map.

$$\boldsymbol{F} : P \to P, \ (u_{20}, u_{30}) \mapsto (u_{21}, u_{31}), \quad (9)$$

$$(u_{21}, u_{31}) = \boldsymbol{F}(u_{20}, u_{30})$$
$$= (f(u_{20}, u_{30}), g(u_{20}, u_{30})). \quad (10)$$

The functions f and g are calculated using Equations (6) and (7).

$$u_{21} = f(u_{20}, u_{30})$$
$$= e^{\delta\tau_0}(-(q - u_{30})\sin\tau_0 + u_{20}\cos\tau_0) \quad (11)$$
$$-p_2(1-q),$$
$$u_{31} = g(u_{20}, u_{30})$$
$$= u_{30}e^{\lambda\tau_0} - p_3(1-q), \quad (12)$$

where the reset time τ_0 is the positive minimum root of the following implicit function.

$$h(u_{20}, u_{30}, \tau_0) = 0$$
$$= e^{\delta\tau_0}((q - u_{30})\cos\tau_0 + u_{20}\sin\tau_0) \quad (13)$$
$$+u_{30}e^{\lambda\tau_0} - 1.$$

Fig.4 shows typical attractors and corresponding to 2-D return maps. Using this map, Lyapunov exponents

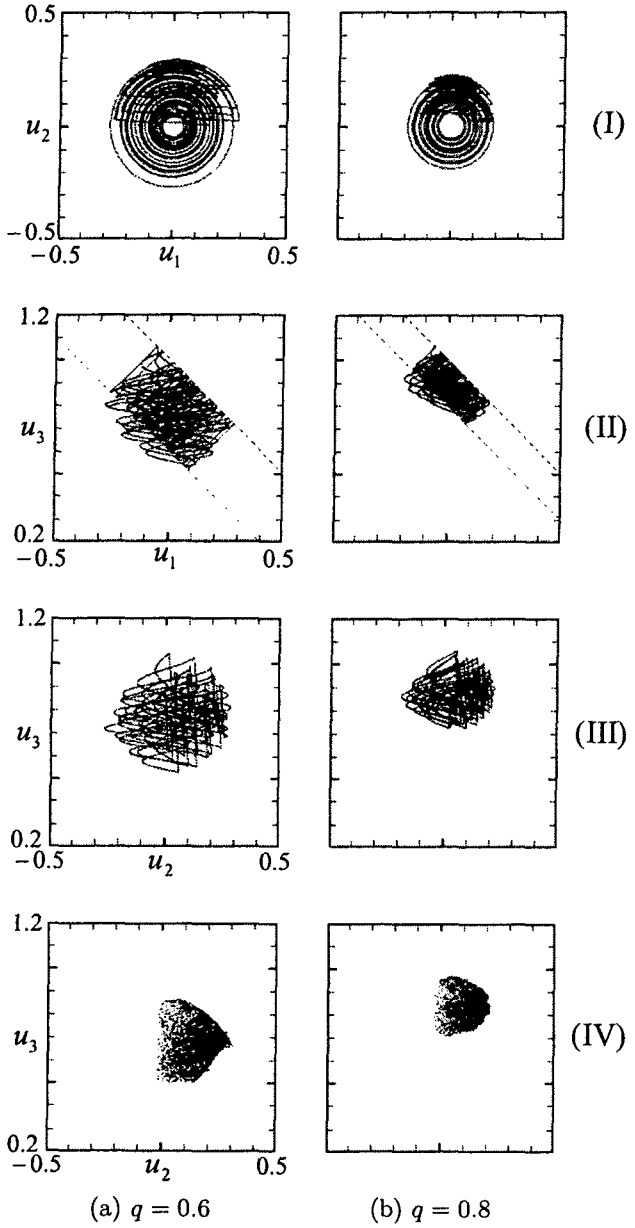

Figure 4. Typical attractors ((I):$u_1 - u_2$ plane, (II):$u_1 - u_3$ plane, (III):$u_2 - u_3$ plane, (IV):2-D return map, $\delta = 0.02$, $\lambda = 0.04$, $p_2 = -0.03$, $p_3 = 0.5$).

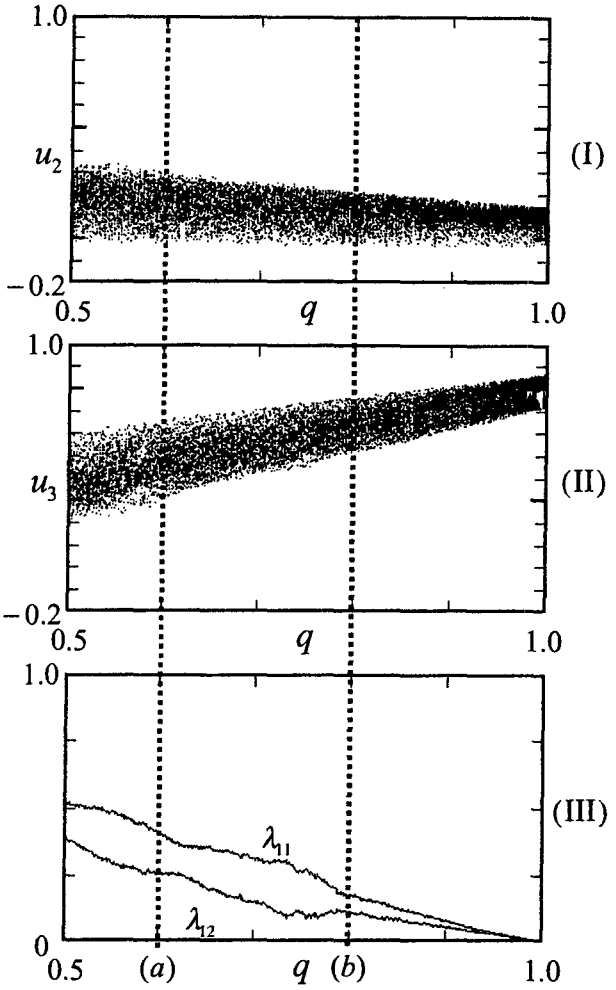

Figure 5. (I), (II) Bifurcation diagrams, (III) Lyapunov exponents ($\delta = 0.02$, $\lambda = 0.04$, $p_2 = -0.03$, $p_3 = 0.5$).

can also be calculated analytically. Fig.5 shows the typical bifurcation diagrams and corresponding to Lyapunov exponents. λ_{11} and λ_{12} denote first and second 1-D Lyapunov exponent, respectively. Since λ_{11} and λ_{12} are positive, the 4-D CSO generates hyperchaos.

4. Laboratory experiments

In this section, we implement the 4-D CSO. The 3PVCCS is constructed by three OTAs. The OTA is realized by the circuit shown in Fig.6(a) with characteristic Fig.6(b). Here, we use a linear region only : $i_o = g(v_{i1} - v_{i2})$. The conductance of the OTA is controlled a resistance $1/g$. The dynamic range of the linear region can be controlled by the saturation current I_{sat} which is adjusted by the bias current I_{CTL}. Threshold voltage is judged using comparator (LM339), switching pulse is generated using mono-stable multi vibrator (4538), and a spiking switch is implemented using analog switch (4066). Fig.7 shows laboratory measurements corresponding to typical attractors shown in Fig.4. The return map attractors can also be observed by inputting the output pulse-train from P.G. in Fig.2 into brightness control terminal (Z-axis) of the oscilloscope.

5. Conclusion

We have presented a novel 4-D chaotic spiking oscillator and a simple implementation circuit. The system can generate hyperchaos characterized by two positive Lyapunov exponents. Using a simple test circuit, we have verified typical phenomena in the laboratory.

Future problems include the analysis bifurcation phenomena for wider parameter region.

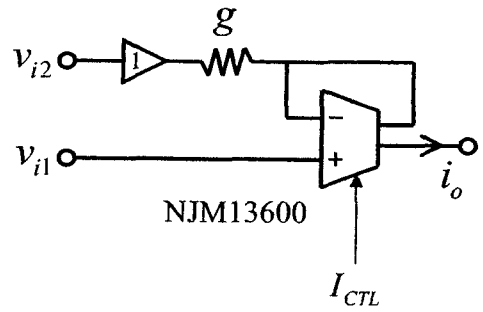

(a) Implementation circuit

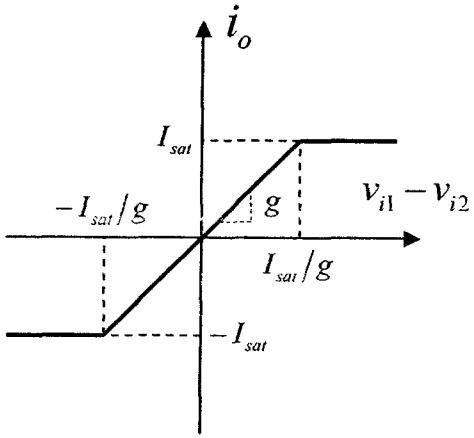

(b) Voltage-current characteristic

Figure 6. Implementation of the OTA.

References

[1] J. P. Keener, F. C. Hoppensteadt, and J. Rinzel, "Integrate-and-fire models of nerve membrane response to oscillatory input," *SIAM J. Appl. Math.*, vol. 41, pp. 503-517, 1981.

[2] H. Nakano & T. Saito, "Basic dynamics from a pulse-coupled network of autonomous integrate-and-fire chaotic circuits," *IEEE Trans. Neural Networks*, vol. 13, pp. 92-100, 2002.

[3] T. Saito, "An approach toward higher dimensional hysteretic chaos generators," *IEEE Trans. Circuits Syst.*, vol. 37, no.3, pp. 399-409, 1990.

[4] T. Suzuki & T. Saito, "On fundamental bifurcations from a hysteresis hyperchaos generator," *IEEE Trans. CAS-I*, 41, no. 12, pp. 876-884, 1994.

[5] E. M. Izhikevich, "Weakly Pulse-coupled oscillators, FM Interactions, Synchronization, and oscillatory associative memory," *IEEE Trans. Neural Networks*, vol. 10, no. 3, pp. 508-526, 1999.

[6] S. R. Campbell, D. Wang and C. Jayaprakash, "Synchrony and desynchrony in integrate-and-fire oscillators," *Neural computation*, vol. 11, pp. 1595-1619, 1999.

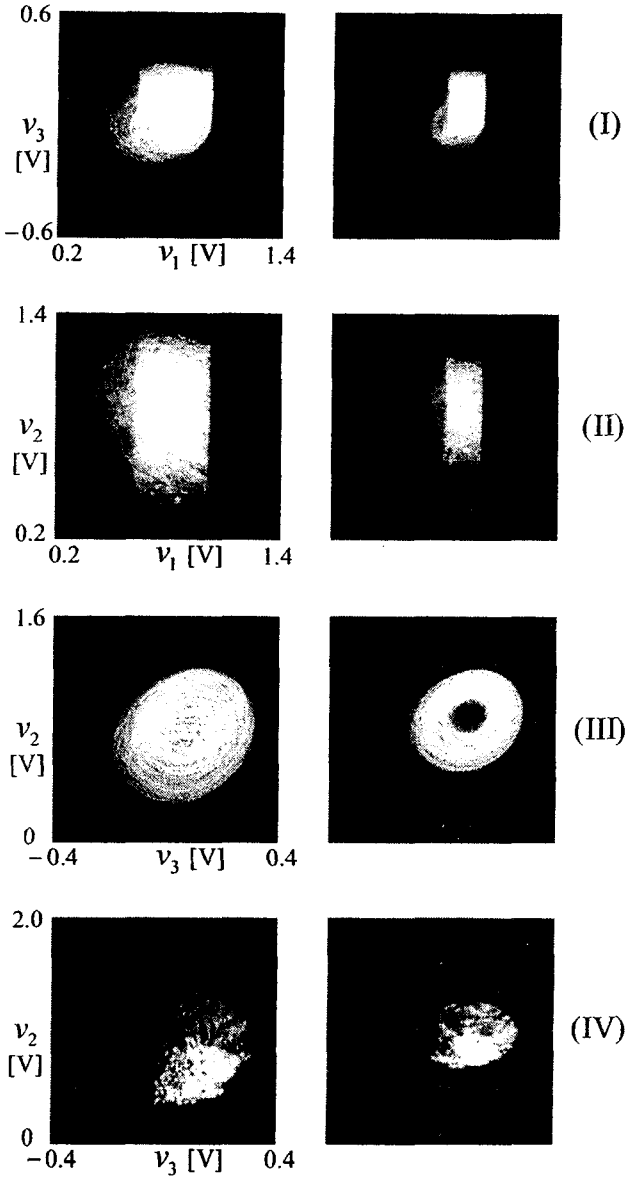

(a) $E \doteq 0.6$[V] (b) $E \doteq 0.8$[V]

Figure 7. Laboratory experiments ((I):$v_1 - v_3$ plane, (II):$v_1 - v_2$ plane, (III):$v_3 - v_2$ plane, (IV):2-D return map, $C_1 \doteq C_2 \doteq C_3 \doteq 2$[nF], $V_T \doteq 1$[V], $1/g_1 \doteq 1/g_2 \doteq 100$[kΩ], $1/g_3 \doteq 1.23$[kΩ]).